## PAPER

Check for updates

# Improving the efficiency of fully hydrocarbon-based proton-exchange membrane fuel cells by ionomer content gradients in cathode catalyst layers†

Hien Nguyen, [ID] ab Dilara Sultanova,b Philipp A. Heizmann, [ID] ac
Severin Vierrath [ID] abc and Matthias Breitwieser*ab

Recently, the cell performances of fully hydrocarbon-based fuel cells approached those of cells with perfluorinated ionomers. Most studies used a low catalyst layer ionomer content (~10 wt%) to enable the highest performance. However, such low ionomer contents can cause a lower cell performance, especially under application-relevant, *i.e.* reduced humidities (≤50% relative humidity). This work systematically investigates ionomer content gradients in cathode catalyst layers based on hydrocarbon ionomer. A graded ionomer content in the catalyst layer with a higher ionomer content in the vicinity of the membrane (I/C = 0.4, 25% of total layer) and a lower ionomer content (I/C = 0.2, 75% of entire layer) near the gas diffusion layer was found to ensure sufficient proton conductivity without compromising reactant transport. In single-cell tests at hot and dry operation conditions ($H_2$/air, 95 °C and 50% RH), the graded layer enabled both significantly improved current density at relevant cell potentials *vs.* a monolithic catalyst layer (496 mA $cm^{-2}$ *vs.* 367 mA $cm^{-2}$@0.7 V) and slightly increased peak performance (0.76 W $cm^{-2}$ *vs.* 0.71 W $cm^{-2}$). Under the given conditions, the performance of the graded layer is similar to that of a Nafion catalyst layer. At 80% RH, the hydrocarbon-graded catalyst layer outperforms the Nafion catalyst layer at high current densities.

## 1. Introduction

The commercialization of fuel cells in the automotive and heavy-duty industry would require a vast amount of perfluorosulfonic acid (PFSA) ionomers, which are state-of-the-art cation exchange materials. The development, production and commercialization of PFSA are limited to a few large chemical companies (*e.g.* Solvay, 3M, Dow, Asahi Kasei Corporation, and Chemours Company) owing to the costly and complex fluorine chemistry. The desired technical goals to higher operating conditions (>100 °C)[1,2] and the mid-term environmental goals to avoid fluorinated materials[3,4] have raised interest in developing alternative and scalable cation exchange materials to PFSA in fuel cell research.

Membranes based on sulfonated phenylated polyphenylene ionomer were reported to enable chemical durability compared to Nafion, *e.g.* 1000 h stability in the accelerated stress test for chemical membrane degradation set by the US Department of Energy.[5,6] However, the performance of hydrocarbon-based fuel cells has so far been inferior to that of Nafion-based fuel cells,[7] and no performance data under application-relevant conditions has been reported. Recently, more works on fluorine-free membrane electrode assemblies (MEAs) for fuel cells have shown performance approaching PFSA-based MEAs.[2,8] Balogun *et al.*[9] have reported a fuel cell based on sulfonated phenylated polyphenylene with performance comparable to Nafion 211 (>1 W $cm^{-2}$ peak power density and 1.2 A $cm^{-2}$ at 0.6 V under $H_2/O_2$ and fully humidified gas). Our previous study[10] demonstrated a fuel cell MEA based on Pemion™ (also based on sulfonated phenylated polyphenylene) with a peak performance that is on par with state-of-the-art PFSA-based MEAs employing short-side-chain materials (>2 W $cm^{-2}$ peak power density and 2.5 A $cm^{-2}$ at 0.6 V under $H_2/O_2$ and fully humidified gas). Despite the promising high performance, all of these reported MEAs were based on monolithic membranes, *i.e.* without a mechanical reinforcement layer, making them most likely inapplicable in actual practice. In addition, the balance of material

*a Electrochemical Energy Systems, IMTEK–Department of Microsystems Engineering, University of Freiburg, Georges-Koehler-Allee 103, 79110 Freiburg, Germany*

*b Hahn-Schickard, Georges-Koehler-Allee 103, 79110 Freiburg, Germany. E-mail: Matthias.Breitwieser@Hahn-Schickard.de*

*c University of Freiburg, Institute and FIT–Freiburg Center for Interactive Materials and Bioinspired Technologies, Georges-Köhler-Allee 105, 79110 Freiburg, Germany*

† Electronic supplementary information (ESI) available. See DOI: https://doi.org/10.1039/d2ma00761d

composition *versus* operation conditions appears even more delicate for fully hydrocarbon-based MEAs than for their typical PFSA-based counterparts. The benchmark performance for fully hydrocarbon-based cathode catalyst layers in our recent work[10] and Balogun *et al.*[9] implied remarkably low ionomer-to-carbon (I/C) ratios of only around 0.2 (∼9 wt% ionomer), enabling the highest overall cell performance. These low I/C ratios were considered the best balance between sufficient gas transports through the inherently more gas-tight hydrocarbon ionomer but allowed still good proton conductivity in the porous electrode. As mentioned in our previous work,[10] in particular, the sensitivity of hydrocarbon MEAs to the humidity of the gas feed makes them not yet applicable under the targeted operation conditions with low humidification.

Lower gas humidification leads to three main problems, which were also observed in PFSA-based systems: lower ORR kinetics,[11,12] higher oxygen transport loss across the ionomer film,[13–15] which in turn also affects the ORR and lower proton conductivity, decreasing the catalyst layer utilization.[12,16–18] While the former problems cannot be quickly resolved by adjusting the ionomer content, the latter can be optimized by an ionomer gradient in the catalyst layer. Theoretical modelling[18,19] and experiments[20–22] suggest an inhomogeneous reaction rate within the catalyst layer. Graded catalyst layers, *i.e.* varying the material composition (*e.g.* Pt on carbon content, ionomer loading, *etc.*) in the catalyst layer through-plane direction, are concepts to address this inhomogeneity. Many works on graded catalyst layers report improved performance, particularly at higher current densities.[19,21–25] These reports raised our interest in transferring the optimized catalyst layer utilization from the Nafion-based systems to hydrocarbon-based catalyst layers. This work uses grading the catalyst layer to have a high ionomer loading only where needed while reducing the loading to improve gas transport. Thus, using a higher I/C ratio close to the membrane, sufficient proton conductivity and an optimized interface to the membrane should be reached. Using a lower I/C ratio near the GDL ensures good gas transport properties.

## 2. Experimental

Pemion™ PP1-HNN8-00-X ionomer (IEC = 3 meq g$^{-1}$, 333 EW) and Pemion™ PF1-HLF9-15-X membranes (IEC = 3 meq g$^{-1}$, 333 EW) were purchased from Ionomr Innovations, Inc. The Pemion™ membrane is a mechanically reinforced membrane with a nominal thickness of 15 μm, which is more suitable for commercial applications due to the higher mechanical stability than the about 8 μm thin monolithic membrane used in our previous report.[10]

### 2.1. Fabrication of membrane electrode assemblies

The stock ionomer solution consists of 5 wt% Pemion™ ionomer and 1:1 w/w isopropanol (IPA)/H$_2$O. The dispersion medium was IPA/H$_2$O (1:1 w/w) and not methanol/water (3:1 w/w) as in our previous report[10] since the performance was not affected (Fig. S1, ESI†) and especially since isopropanol has less severe

toxicity than methanol. The ionomer stock solution is stirred at 40 °C and 200 rpm for at least 12 hours to ensure complete dissolution. The stock solution is added to the ink, consisting of the catalyst powder and the 1:1 w/w IPA/H$_2$O dispersion medium. The solid content of the catalyst inks was kept at 0.95 wt%.

The catalyst used in the anode catalyst layer (CL) is Pt/C (45.3 wt% Pt content, Elyst Pt50 0550, Umicore), while that used in the cathode catalyst layer is PtCo/C (45.3 wt% Pt content, Elyst Pt50 0690, Umicore). Cathode catalyst inks are prepared following the same procedure as for the anode. The dry ionomer content in the anode CL is 14 wt%, corresponding to an I/C of 0.3. Cathode catalyst inks with various I/C ratios (0.1 to 0.5) are used to systematically investigate the effect of graded ionomer content in the CL.

Nafion (D2020, DuPont) was used as the binder in the anode and cathode as a reference for the best gradient hydrocarbon-based catalyst layers (Section S3.3, ESI†). The Nafion anode CL contains Pt/C (45.3 wt% Pt content, Elyst Pt50 0550, Umicore) and a dry ionomer content of 33 wt%, as reported in the literature (30–33 wt%).[9,21] The Nafion ionomer content used in the PtCo/C cathode CL was varied from 0.3 to 0.9. An ionomer content of 25 wt% (I/C = 0.6) was found to be optimum for the operating conditions (95 °C, 50% and 80% RH, 250 kPa$_{abs}$, Section 2.2) and, thus, provides the fairest benchmark for the hydrocarbon gradient catalyst layers.

The catalyst inks are deposited on the pristine Pemion™ membranes with an ultrasonic spray system (Sonaer Sono-Cell). Fabricating the membrane electrode assemblies is identical to our previously reported study.[10] The aimed Pt loading for the anode is 0.1 mg cm$^{-2}$, and the total Pt loading for the cathode is 0.4 mg cm$^{-2}$. The Pt loading was controlled during the spray coating procedure by weighing a thin metal pad of a 2 cm$^2$ area before and after spraying with a microbalance (ME36S, Sartorius AG). The final Pt loading was confirmed by micro X-ray fluorescence spectroscopy (μXRF, Bruker Tornado M4).

In the first part of this work, different ionomer contents within the graded catalyst layers were tested in a proportion of 25% of the total Pt loading in the catalyst layer (0.1 mg$_{Pt}$ cm$^{-2}$) to the membrane (sub-layer I, Fig. 2) and 75% of the total Pt loading (0.3 mg$_{Pt}$ cm$^{-2}$) towards the gas diffusion layer (sub-layer II, Fig. 2). High I/C ratios were chosen for sub-layer I (0.4 or 0.5), and lower I/C ratios (0.2 or 0.1) were kept for sub-layer II. After comparing the two graded cathode catalyst layers (0.4/0.1 *vs.* 0.4/0.2), the graded cathode catalyst layer with higher I/C to the membrane (0.5/0.2) is also tested.

The second part investigated the proportion of the two sub-layers with the best combination of the I/C ratios. The sub-layer I to sub-layer II ratio was increased from 0% (pure sub-layer II) to 25% of sub-layer I/75% of sub-layer II to 50% of sub-layer I/50% of sub-layer II to 100% of pure sub-layer I.

### 2.2. Electrochemical characterization

The *in situ* performances of the MEAs were evaluated by a fuel cell testing system (Scribner 850e). Freudenberg (H14Cx653) GDL substrates were used. The protocol applied to all MEAs begins with a break-in procedure described in our previous

work,[10] followed by the mass activity measurement ($H_2/O_2$ polarisation curve under 80 °C, 96% RH and 150 $kPa_{abs}$).

The mass activities of catalyst layers were investigated under set conditions by the US Department of Energy (DOE);[26,27] $H_2/O_2$ polarisation curves (0.25 slpm/1 slpm) were measured under 80 °C, 96% RH and 150 $kPa_{abs}$. The current density was scanned from 0 mA cm$^{-2}$ to 125 mA cm$^{-2}$ in 5 mA cm$^{-2}$ steps for 5 minutes per point (average of last 5 seconds used). The $H_2/O_2$ polarisation curves for the mass activity determination were corrected for membrane, contact and electronic resistances, represented by the high-frequency resistances (HFRs). The HFRs were measured simultaneously with the polarization data and were used to evaluate the membrane, interfacial and electronic resistances. HFR spectra were recorded at a frequency of 3200 Hz by the Frequency Resistance Analyzer (FRA) integrated into the fuel cell testing hardware, as described in our earlier work.[10] To correct the hydrogen cross-over current densities for the mass activity evaluation, linear sweep voltammetry (LSV) was conducted under $H_2/N_2$ (0.2/0.05 l min$^{-1}$), 80 °C, 96% RH and 150 $kPa_{abs}$. The Tafel plots were corrected for the ohmic resistance and the hydrogen cross-over current densities $i_{x\text{-over}}$ following the approach by Neyerlin et al.[18] The mass activity is obtained by dividing the current density corrected with hydrogen cross-over ($i + i_{x\text{-over}}$) at 0.9 $V_{HFR\text{-free}}$ and normalized with the cathode Pt-loading of the cell (0.4 $mg_{Pt}$ cm$^{-2}$), which is verified by the micro X-ray fluorescence spectroscopy (μXRF).

The cyclic voltammograms (CVs) were measured under $H_2/N_2$, 35 °C, 96% RH and ambient pressure. The potential was swept from 0.05 to 1.0 V versus RHE at a scan rate of 50 mV s$^{-1}$. The CVs were repeated 8 times to reach saturation. As reported in the literature,[7,25] the factor used to calculate the ECSA from the $H_{upd}$ charge was 210 μC cm$^{-2}$. Note that the hydrogen underpotential deposition ($H_{upd}$) for Pt-alloy only serves as an indicative value for ECSA due to the altered structural and electronic properties of PtCo, which impact the adsorption behaviour of hydrogen.[28–30] A LSV under the same conditions as the CV ($H_2/N_2$, 35 °C, 95% RH and ambient pressure) was additionally recorded after the CVs to correct possible electrical shorts.

$H_2$/air polarisation curves (0.25 slpm/1 slpm) under commercial applications relevant conditions: $H_2$/air, 95 °C and 250 $kPa_{abs}$ were measured under two different humidities: (a) 50% RH and (b) 80% RH. The current density was scanned from zero to 250 mA cm$^{-2}$ in 12.5 mA cm$^{-2}$ increments with a 1 minute hold at each current step.[10] Afterwards, the current densities were scanned from 375 mA cm$^{-2}$ to 6250 mA cm$^{-2}$ in 125 mA cm$^{-2}$ increments with a 3-minute hold per current step.[10]

The proton resistance in the catalyst layers at 50% RH and 96% RH was characterized via AC impedance spectroscopy (Gamry Interface 5000E) recorded in $H_2/N_2$ at 0.45 $V_{DC}$ with a root-mean-square perturbation of 1.75 mV between 100 kHz and 0.2 Hz (20 points per decade). The impedance spectroscopy was performed with high flow rates of $H_2$ and $N_2$ (0.5 slpm/0.5 slpm) to avoid possible artefacts caused by mass transport limitations. The cells operated in the same conditions as the

mass activity measurements, i.e. 80 °C and 150 $kPa_{abs}$. The measurements started at low RH to ensure the validity of the proton resistances at lower humidity since the rest water from the previous experiment with higher humidity could remain in the pores of the catalyst layers and positively affect the proton resistances at lower humidity.

### 2.3. Scanning electron microscopy (SEM)

SEM images of the focused ion beam (FIB)-cut cross-sections were acquired with a FE-SEM Amber X (Tescan GmbH) at 2 kV acceleration voltage. The working distance was 6 mm, and the beam current was 100 pA. An inclined-positioned Everhart–Thornley (ET) detector was used to acquire the images. To quantitatively determine the layer thicknesses, the SEM images obtained were tilt-corrected and analyzed using ImageJ 1.53c. The catalyst layer was segmented using "Trainable Weka Segmentation", a machine learning-based plugin.[31] This allows rapid and accurate segmentation of CLs that are non-homogeneous from an image-processing perspective. The final binary segmented images were then evaluated via MatLab, and the obtained layer thicknesses were binned in 0.25 μm units for visualization purposes. Both the obtained SEM images and the respective CL thickness histograms are presented in the ESI.†

### 2.4. Micro X-ray spectroscopy (μXRF)

The Pt loading in the cathode CL was characterized by the micro X-Ray fluorescence (μXRF). Simultaneously to membrane coating, the CL ink was deposited on a GDL (H14Cx653, Freudenberg). The reported Pt loading is the average Pt loading of the gas diffusion electrode (GDE) over its area (2 cm$^2$). The Pt-loading was characterized by the area analysis mode, i.e. multiple single-point analyses scanned over the area of the GDL. The current density was 600 μA, and the measurement time was 30 seconds per point. The resolution of the XRF was 60 μm.

## 3. Results and discussion

The effects of Nafion content in the catalyst layer were studied extensively:[32–35] A catalyst layer with a low ionomer content (<25 wt%)[32,35] has a lower proton conductivity but facilitates oxygen transport. In contrast, a higher ionomer content (>30 wt%) provides good proton conductivity but affects mass transport.[32,35] An optimized Nafion ionomer content in the CLs has a well-balanced proton conductivity and mass transport under a wide range of humidities (50–100% RH).

For hydrocarbon-based MEAs, similar trends apply: a delicate balance between proton conductivity and oxygen transport is required to achieve optimal performance.[9] Due to the higher swelling and the lower gas permeability of typical hydrocarbon ionomers compared to PFSAs, this balance is even more critical for hydrocarbon ionomers. At high humidity (>50% RH), a lower ionomer content (<10 wt%) seems sufficient for sufficient proton conductivity in the catalyst layer due to its relatively high ion exchange capacity (IEC) and high swelling. A higher ionomer
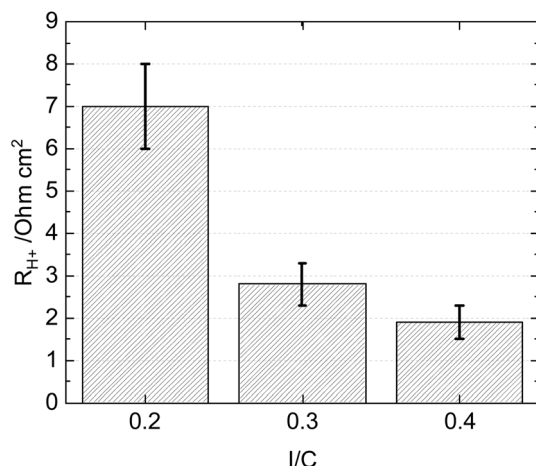
**Fig. 1** Proton resistance of MEAs with different cathode I/C ratios (mono-layers). The $H_2/N_2$ impedance spectroscopy is measured at 80 °C, 50% RH and 150 $kPa_{abs}$.
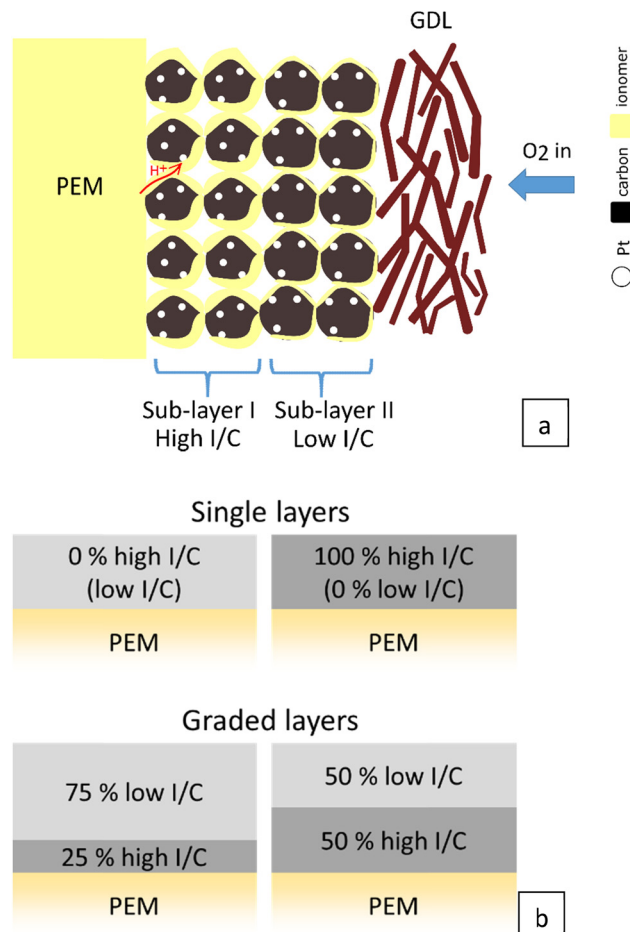


**Fig. 2** Schematic illustration of the cathode catalyst layer with ionomer content gradient (a) and the proportion variation of sub-layer I (high I/C) and sub-layer II (low I/C) (b).

content is desired at low humidity for good proton conductivity or CL utilization.[18] Fig. 1 confirms the higher proton conductivity of a CL with the higher ionomer content (I/C = 0.4 or 18 wt%) compared to that with lower ionomer content (I/C = 0.2 or 9 wt%) at 50% RH.

However, a high ionomer content has detrimental effects on oxygen diffusion in the CL due to hydrocarbon ionomers' inherent low gas permeability.[7,36] Furthermore, a high ionomer content can cause increased catalyst poisoning by sulfonate[37,38] or phenyl groups[39–41] or provoke catalyst layer flooding due to the increased CL's hydrophilicity induced by the high ion exchange capacity of the ionomer. All of these factors have undesirable impacts on the overall performance of the fuel cells.

Ionomer gradients have been shown for Nafion catalyst layers to improve performance at high current densities.[21,22,24] In these studies,[21,22] the optimal ionomer content near the membrane was between 30 and 40 wt% and around 20 wt% near the gas-diffusion media. The improved performance was explained by better proton conductivity at the catalyst layer/membrane interface[22] and better mass transport[22] or a reduction of flooding problems[21] at the catalyst layer/gas diffusion medium interface.

In our previous study,[10] the optimal I/C ratio was 0.2 since the best compromise to enable cell operation to high current and power densities. However, limitations have been encountered at application-relevant cell voltages >0.6 V. This encouraged optimizing the MEAs with an I/C higher than 0.2 owing to the higher proton conductivity, especially at low humidity. With a graded catalyst layer, the higher I/C ratio can be partially utilized in the CL without sacrificing performance at high current densities. A schematic illustration of the cathode catalyst layer with a graded ionomer and the proportion variation between high I/C and low I/C are shown in Fig. 2.

The following investigated the optimal graded ionomer content and its proportion in the catalyst layer. The I/C in the sub-layer I (Pt Loading = 0.1 $mg_{Pt}$ $cm^{-2}$) was kept at 0.4, as the proton resistance of the homogeneous CL with this ionomer content was the lowest at 50% RH (Fig. 1).

### 3.1. Effects of ionomer content of the graded catalyst layer

Under fully humidified conditions, the mass activities and the electrochemical active surface areas (ECSAs) of the MEAs with pure cathode I/Cs (0.2 and 0.4) are similar to those of MEAs with graded CLs (Table 1). The cyclic voltammograms of all cells are shown in Fig. S2a (ESI†). The Tafel plots and the loading-corrected mass-specific current densities of all samples are extracted from the HFR-corrected data $E_{HFR-free}$ (Fig. S3a and b, ESI†).

The highest proton resistances are those of the CL, with an I/C of 0.2 and 0.4/0.1. The standard deviation of the proton resistance of the CL with the I/C = 0.4/0.1 is comparably high (> ±50%). This deviation could be linked to the too-low ionomer content in the catalyst layer (I/C < 0.2).

The thicknesses of MEAs with graded catalyst layers are similar to those of MEAs with homogeneous CLs (between 9 and 11 μm). The thickness of the CL with the I/C = 0.2 is slightly lower than those of the rest. As a result, the thickness does not significantly affect the trend in proton resistivity (quotient of the CL proton resistance and thickness). The cross-sections of the CLs are shown in Fig. S5a–f (ESI†), along with thickness histograms (Fig. S6a–f, ESI†).

**Table 1** Mass activities, proton resistances, Tafel slopes, cathode CL thicknesses and Pt-loading of MEAs with different ionomer content in the outer CL (GDL). The electrochemical properties are tested under 80 °C, $H_2/O_2$, 96% RH and 150 $kPa_{abs}$

| $I/C_{PEM}$ (0.1 mg cm$^{-2}$) (25%)/$I/C_{GDL}$ (0.3 mg cm$^{-2}$) (75%) | Mass activity in A g$^{-1}$ | Tafel slopes in mV dec$^{-1}$ | Proton resistances in mOhm cm$^2$ | Cathode CL thickness in μm | Proton resistivity in Ohm cm | ECSA in m$^2$ g$^{-1}$ | Cathode Pt loading in mg cm$^{-2}$ |
|---|---|---|---|---|---|---|---|
| 0.2/0.2 | 58 ± 4 | 83 ± 10 | 108 ± 72 | 8.7 ± 0.7 | 124 | 29 ± 2 | 0.42 |
| 0.4/0.4 | 66 ± 2 | 85 ± 1 | 81 ± 3 | 9.1 ± 0.4 | 89 | 35 ± 2 | 0.43 |
| 0.4/0.2 | 65 ± 7 | 86 ± 3 | 80 ± 4 | 10.2 ± 0.8 | 78 | 31 ± 2 | 0.43 |
| 0.4/0.1 | 68 ± 5 | 99 ± 5 | 200 ± 100 | 10.7 ± 0.9 | 228 | 30 ± 1 | 0.46 |
| 0.5/0.2 | 62 ± 3 | 82 ± 5 | 57 ± 9 | 9.8 ± 0.5 | 58 | 28 ± 1 | 0.45 |

The proton resistivity of the graded CL with the I/C = 0.4/0.1 is substantially higher than the rest (228 Ohm cm), which is expected due to the lower ionomer amount. As the Tafel slopes are extracted from the corrected cell voltage to the high-frequency resistance $E_{HFR\text{-}free}$, they can be greater due to very high proton resistances.[18] While the voltage losses to proton resistance are negligible in the Tafel slopes of the other ME, the Tafel slope of the MEA with the 0.4/0.1-graded CL is slightly higher, which is likely affected by the voltage losses due to its proton resistance. The proton resistivity of the cathode I/C = 0.5/0.2 is even lower than that of the CL with pure I/C = 0.4. In addition, the increased ionomer content from 0.2 to 0.4 of only 25% of the total cathode Pt loading in the vicinity of the membrane (sub-layer I) reduces the proton resistivity of the graded ionomer CL to the range of the pure I/C = 0.4 (80–90 Ohm cm). These results imply the importance of proton conductivity in the vicinity of the membrane|CL interface.

The polarization behaviour of the MEAs with the single- and graded layers was characterized under hot and dry conditions relevant for heavy-duty applications and aviation (95 °C, 50% RH and 250 $kPa_{abs}$). The performance of the 0.4/0.2-graded CL MEA was increased by 35% at 0.7 V compared to the MEAs with homogeneous cathodes I/C (0.2 and 0.4) under the given conditions (Fig. 3).

The higher performance of the graded CL (I/C = 0.4/0.2) compared to that of the CL with I/C = 0.4 is attributed to the lower ionomer content at the GDL side of the CL, which potentially has better oxygen transport. This result is similar to the observations in previous studies with Nafion.[21,22] Compared to the MEA with the graded cathode CL of 0.4/0.1, the MEA with the cathode I/C = 0.4/0.2 enables higher performance, most likely attributed to the significantly higher proton conductivity of sub-layer II (Fig. S7, ESI†). Despite the very low proton conductivity in the graded 0.4/0.1 CL, it is remarkable that the cell performance of the MEA with the cathode I/C = 0.4/0.1 is still higher than that with the pure cathode I/C = 0.4, especially at $E < 0.6$ V (Fig. 3). The result is remarkable, as it might indicate that sufficient oxygen transport, especially at the outer CL (to the GDL), appears to be more critical than the proton conductivity at high current densities.

The performance of the MEA with the graded cathode I/C = 0.4/0.2 is also higher than that with the graded cathode I/C = 0.5/0.2, despite the higher proton resistivity (Table 1). The difference is attributed to the higher I/C of the sub-layer I (PEM), which likely affects oxygen diffusion. The higher performance of the MEA with graded cathode I/C = 0.5/0.2 compared
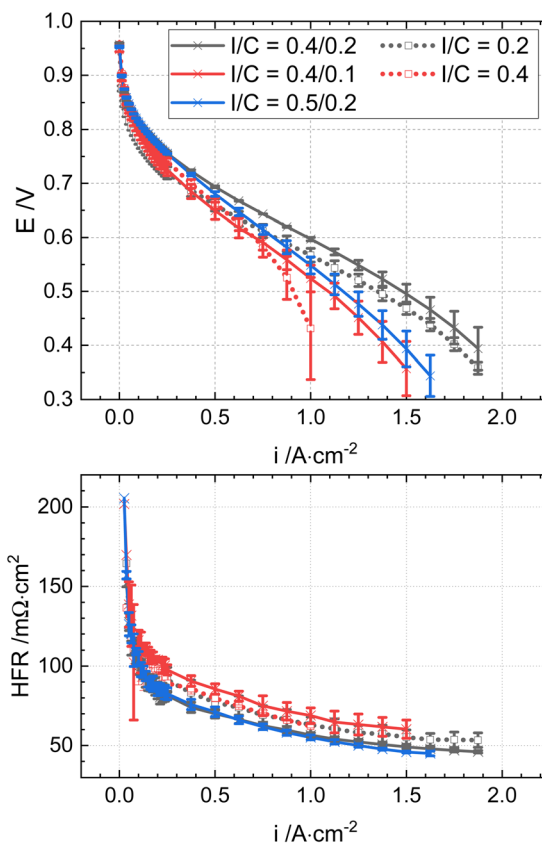


**Fig. 3** Polarization curves of MEAs with pure I/C = 0.2 and 0.4 (dot lines) and cathode graded I/C rations (solid lines): 0.4/0.2, 0.4/0.1 and 0.5/0.2. Test conditions: $H_2$/air, 95 °C, 50% RH, 250 $kPa_{abs}$.

to that with the graded cathode I/C = 0.4/0.1 is probably linked to the lower losses to proton resistivity over the complete CL. The impeded oxygen transport in sub-layer I of the graded cathode I/C = 0.5/0.2 might be less impactful on the overall performance than the lack of proton conductivity in sub-layer II of the cathode I/C = 0.4/0.1 (compared to cathode I/C = 0.4/0.2) (Fig. 3).

### 3.2. Effect of catalyst layer composition

Given the optimal I/C of the graded CL (0.4/0.2), the first and second sub-layer ratio was changed from 25%/75% to 50%/50%. These graded layers were compared to single layers with I/Cs of 0.2 and 0.4 (Table 2).

According to Neyerlin *et al.*,[18] the voltage loss due to proton resistances is negligible if the ratio of proton transport

**Table 2** Mass activities, proton resistances, Tafel slopes, cathode CL thicknesses and Pt-loading of MEAs with different proportions of CL with I/C = 0.4 (0%, 25%, 50% and 100%). The electrochemical properties are tested under 80 °C, $H_2/O_2$, 96% RH and 150 $kPa_{abs}$

| I/C | Mass activity in A $g^{-1}$ | Tafel slopes in mV $dec^{-1}$ | Proton resistances in mOhm $cm^2$ | Cathode CL thickness in μm | Proton resistivity in Ohm cm | ECSA in $m^2$ $g^{-1}$ | Cathode Pt loading in mg $cm^{-2}$ | $iR_{H^+}$/Tafel slope |
|---|---|---|---|---|---|---|---|---|
| 100 % 0.2 | 58 ± 4 | 83 ± 10 | 108 ± 72 | 8.7 ± 0.7 | 124 | 29 ± 2 | 0.42 | 0.03 ± 0.02 |
| 25 % 0.4 75 % 0.2 | 65 ± 7 | 86 ± 3 | 80 ± 4 | 10.2 ± 0.8 | 78 | 31 ± 2 | 0.43 | 0.0254 ± 0.0002 |
| 50 % 0.4 50 % 0.2 | 61 ± 5 | 90 ± 1 | 129 ± 15 | 10.1 ± 0.8 | 128 | 28 ± 1 | 0.45 | 0.039 ± 0.001 |
| 100 % 0.4 | 66 ± 2 | 85 ± 1 | 81 ± 3 | 9.1 ± 0.4 | 89 | 35 ± 2 | 0.43 | 0.027 ± 0.002 |

resistance over kinetic resistance ($iR_{H^+}$/Tafel slope) is less than 0.15.[18] In this study, the ratios $iR_{H^+}$/Tafel slope of all MEAs are below 0.15 (Table 2), assuring negligible voltage losses due to proton resistance and a reasonable low current density ($<100$ mA $cm^{-2}$) for the evaluation of the ORR kinetics.[18]

Similar mass activities (60–70 A $g^{-1}$), ECSAs (30–35 $m^2$ $g^{-1}$) and Tafel slopes (80–90 mV $dec^{-1}$) were observed for all samples, indicating no differences in the kinetics of the four cells at 80 °C, 96% RH and 150 $kPa_{abs}$. The mass activities of the hydrocarbon-based cells were reported to be generally lower than the typical values of PFSA-based cells ($\gg 70$ A $g^{-1}$),[10,42,43] despite applied I/C- and graded ionomer content optimization. As mass transport limitations should be negligible under these conditions ($H_2/O_2$ and 150 $kPa_{abs}$) and low current densities ($<100$ mA $cm^{-2}$),[44] the lower mass activity could be related to the ORR kinetics. The lower mass activity thus might be linked to the excessive amount of sulfonate groups in the hydrocarbon ionomer poisoning the catalyst.[37] The Tafel plots (Fig. S4a, ESI†), the mass-specific current density (Fig. S4b, ESI†) and the cyclic voltammograms (Fig. S2b, ESI†) show no difference in these values.

Fig. 4 shows the proton resistance and resistivity at 80 °C and 50% RH. The proton resistances and resistivity are remarkably reduced by the increasing proportion of I/C = 0.4. This observation

emphasizes the importance of proton conductivity of hydrocarbon-based CL next to the membrane at low humidity operations, which can be explained by the higher current distribution next to the membrane at lower humidity.[18]

Fig. 5 shows the polarisation curves of the four cells and the Nafion reference cell under 95 °C, 50% RH, and 250 $kPa_{abs}$. The MEAs with CLs with higher I/C (0.4) at the PEM yield higher performance at E > 0.75 V than that with pure cathode I/C = 0.2 (0% of I/C = 0.4). The MEAs with CL with the higher proportion of the I/C = 0.2, i.e. 0% - 25% of I/C = 0.4, in the sub-layer II yield higher performance at E < 0.6 V than the other cells with a lower proportion. The MEA with the cathode I/C = 0.4 (100%) has the lowest performance at E < 0.6 V, most likely due to the limited oxygen transport and flooding.

The performance at 0.7 V of the 25% (I/C = 0.4) graded cathode CL was improved by 35% compared to that with pure cathode I/C = 0.2 and became in line with the Nafion reference under the given conditions. Increasing the I/C = 0.4 proportion of the CL to 50% leads to a decrease in the overall performance. These results show that a higher ionomer content (25% of the CL total Pt loading) in the vicinity of the membrane is beneficial for the low current density region, and it is essential to keep the ionomer content low in the vicinity of the GDL (>50% of the CL total Pt loading) for the high current density region to reduce oxygen resistance. Consequently, the CL with higher amounts of ionomer close to the membrane and less close to the GDL performs best throughout the current density range. The optimal proportion of the low I/C catalyst layer in hydrocarbon cells (75% of the total catalyst layer thickness) is higher than that of Nafion cells (~30% of the total Nafion catalyst layer thickness).[21,22] This result confirms proton conductivity and oxygen permeability differences between hydrocarbon and Nafion ionomers.

At high humidity (80%, Fig. 6), the beneficial properties of the cell with 25% I/C of 0.4 are maintained but less expressed as under 50% RH. The performance of the optimal gradient ionomer cell is in the range of the Nafion cell under low current densities ($i < 1.4$ A $cm^{-2}$) and outperforms the Nafion cell at higher current densities ($i > 1.4$ A $cm^{-2}$). The current densities at 0.7 V and the peak power densities of the MEAs are shown in the bar chart in Fig. 6c. The performance of the MEA with 25% (I/C = 0.4) graded cathode CL is also higher than the rest at 80% RH, but the improvement compared to, e.g. the MEA with pure I/C = 0.2 was ~20%, which is not as significant as the improvement at 50% RH (~35%).
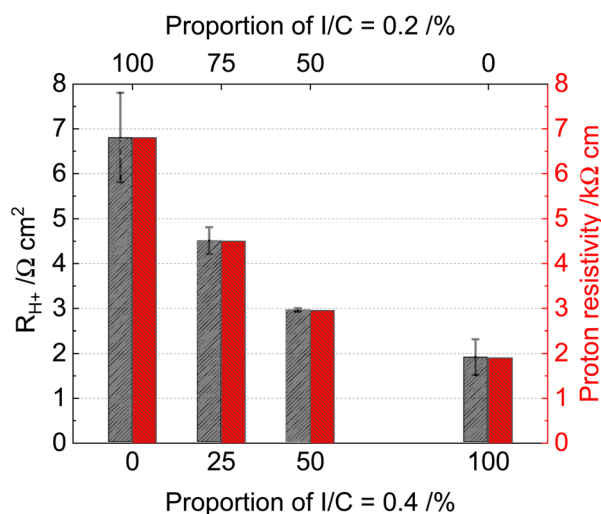


**Fig. 4** Proton resistance and proton resistivity of the MEAs with an increasing proportion of cathode I/C = 0.4 (0% of I/C = 0.4 corresponds to a pure cathode I/C = 0.2). Test conditions: 80 °C, 50% RH, 150 $kPa_{abs}$.
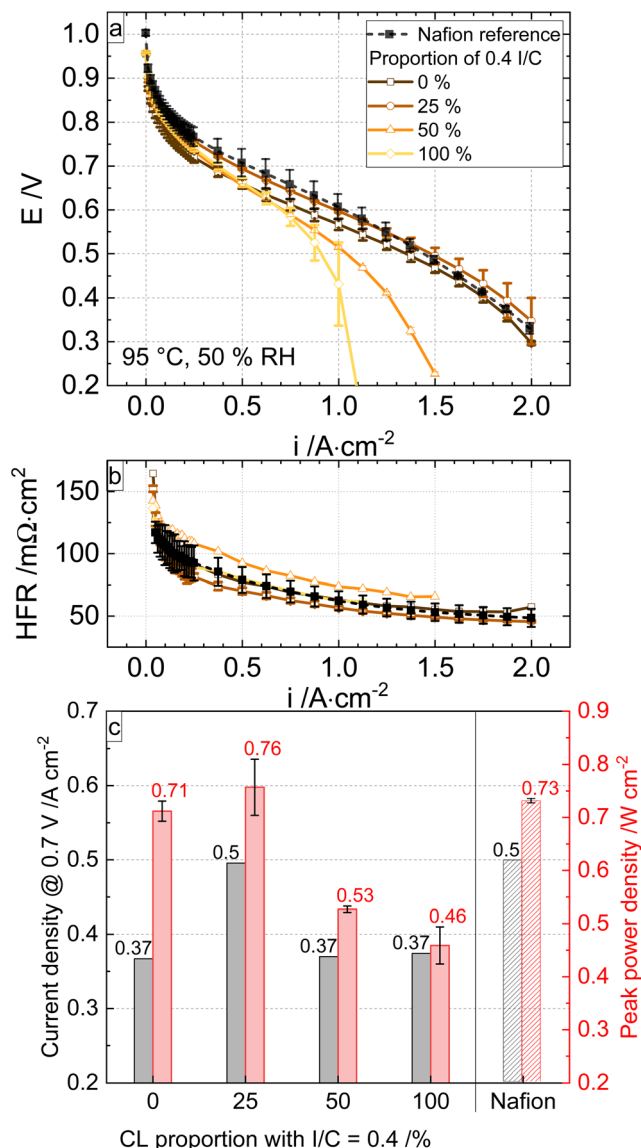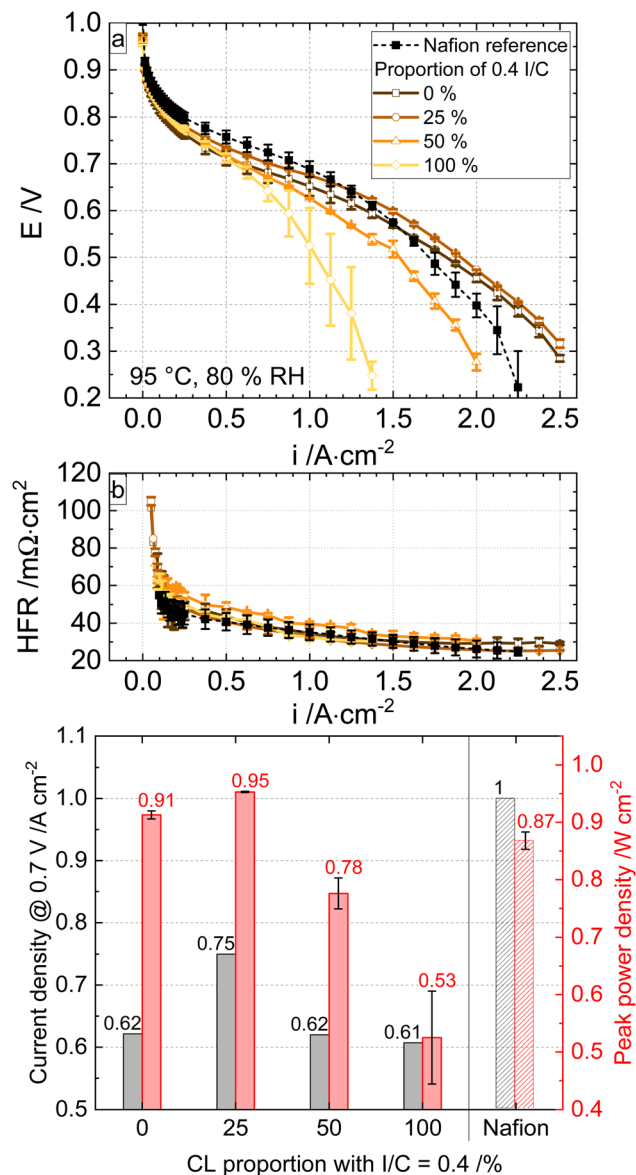
**Fig. 5** Polarization curves (a), HFRs (b) and extracted current densities at 0.7 V and peak power densities (c) of the Nafion reference and the hydrocarbon MEAs with proportions of cathode I/C = 0.4 (at the PEM|CL) varying from 0% I/C = 0.4 (100% I/C = 0.2) to 100% I/C = 0.4. Testing conditions: $H_2$/air, 95 °C, 50% RH, 250 kPa$_{abs}$.



**Fig. 6** Polarization curves (a), HFRs (b) and extracted current densities at 0.7 V and peak power densities (c) of the Nafion reference and the hydrocarbon MEAs with proportions of cathode I/C = 0.4 (at the PEM|CL) varying from 0% I/C = 0.4 (100% I/C = 0.2) to 100% I/C = 0.4. Testing conditions: $H_2$/air, 95 °C, 80% RH, 250 kPa$_{abs}$.

The metrics of a current density of 750 mA cm$^{-2}$ at 0.7 V and an improved peak performance of 0.95 W cm$^{-2}$ (95 °C, 80% RH) are a new benchmark for fully hydrocarbon MEAs with commercially available and mechanically reinforced hydrocarbon membranes. The gradient system with 25/75% of I/C 0.4/0.2 enabled the highest peak performance and current density at 0.7 V cell voltage under dry and wet conditions.

## 4. Conclusion

This work systematically investigates catalyst layers with ionomer gradients for fully-hydrocarbon-based fuel cell MEAs. It is found that a higher I/C ratio close to the membrane and lower

I/C at the GDL side enables higher performance compared to the single I/C in the catalyst layer. This concept of catalyst layer design is a simple way to circumvent inhomogeneous ORR current distribution in the CL at low humidity.[18] This finding is in line with previous studies on PFSA-based MEAs.[21,22,25] For hydrocarbon-based MEAs, however, the impact of the gradients on the overall performance is more pronounced than for previous reports with PFSA,[21,22] especially at low humidity. Compared to homogeneous cathodes I/C (0.2 and 0.4), we observed increased performance at 0.7 V cell voltage by up to 35% with the optimal graded ionomer cathode: I/C = 0.4 in the 25% close to the membrane, 0.2 in the remaining 75% of the catalyst layer. It is believed that the improvement is attributed

to a reduction of proton resistivity and, thus, a better CL utilization at low humidity (50% RH) without compromising oxygen transport and, therefore, also allowing high cell performance at high current densities. The optimized gradient ionomer cathode performance is comparable to a Nafion-based catalyst layer in both application-relevant voltage ranges (0.8–0.65 V) and maximum power density. The optimized composition of 25% 0.4 I/C and 75% 0.2 I/C in the cathode CL confirms this delicate balance between proton conductivity and reactant transport. This finding improves achievable current densities at relevant cell potentials *versus* a monolithic catalyst layer (496 mA cm$^{-2}$ *vs.* 367 mA cm$^{-2}$ at 0.7 V) while maintaining peak performance (0.76 W cm$^{-2}$ *vs.* 0.72 W cm$^{-2}$). Future work will focus on further refinement of graded catalyst layers to improve the performance of fully hydrocarbon-based fuel cells and reduce the Pt loading. The concept of a graded ionomer CL could be transferred to low Pt loading cells to enhance their performance. It also remains to clarify whether and to what extent the currently observed limitations in PFSA-based cathodes with low Pt-loading[45] apply to optimized hydrocarbon catalyst layers. Moreover, it is essential to investigate the durability of the optimized hydrocarbon catalyst layers.

## Conflicts of interest

There are no conflicts of interest to declare.

## Acknowledgements

## References

1 T. Suzuki, A. Iiyama, N. Kubo, N. Saito, K. Shinohara, S. Shimotori, Y. Sugawara and K. Yamada, (Invited) Toward the Future Fuel Cell-Challenge for 2040, *ECS Trans.*, 2019, 3–7.

2 H. Nguyen, C. Klose, L. Metzler, S. Vierrath and M. Breitwieser, Fully Hydrocarbon Membrane Electrode Assemblies for Proton Exchange Membrane Fuel Cells and Electrolyzers: An Engineering Perspective, *Adv. Energy Mater.*, 2022, **12**, 2103559.

3 European chemical agency. Five European states call for evidence on broad PFAS restriction. **https://echa.europa.eu/de/-/five-european-states-call-for-evidence-on-broad-pfas-restriction** (accessed October 25, 2021).

4 The Organisation for Economic Co-operation and Development. Reconciling Terminology of the Universe of Per- and Polyfluoroalkyl Substances: Recommendations and Practical Guidance. **https://www.oecd.org/chemicalsafety/portal-perfluorinated-chemicals/terminology-per-and-polyfluoro-alkyl-substances.pdf**.

5 S. Xu, M. Adamski, M. Killer, E. M. Schibli, B. J. Frisken and S. Holdcroft, Sulfo-Phenylated Polyphenylenes Containing Sterically Hindered Pyridines, *Macromolecules*, 2019, **52**, 2548–2559.

6 M. Adamski, T. J. G. Skalski, B. Britton, T. J. Peckham, L. Metzler and S. Holdcroft, Highly Stable, Low Gas Crossover, Proton-Conducting Phenylated Polyphenylenes, *Angew. Chem., Int. Ed.*, 2017, **56**, 9058–9061.

7 J. Peron, Z. Shi and S. Holdcroft, Hydrocarbon proton conducting polymers for fuel cell catalyst layers, *Energy Environ. Sci.*, 2011, **4**, 1575.

8 C. Klose, T. Saatkamp, A. Münchinger, L. Bohn, G. Titvinidze, M. Breitwieser, K.-D. Kreuer and S. Vierrath, All-Hydrocarbon MEA for PEM Water Electrolysis Combining Low Hydrogen Crossover and High Efficiency, *Adv. Energy Mater.*, 2020, **10**, 1903995.

9 E. Balogun, M. Adamski and S. Holdcroft, Communication—Non-Fluorous, Hydrocarbon PEMFCs, Generating > 1 W cm $-2$ Power, *J. Electrochem. Soc.*, 2020, **167**, 84502.

10 H. T. T. Nguyen, F. Lombeck, C. Schwarz, P. A. Heizmann, M. Adamski, H.-F. Lee, B. Britton, S. Holdcroft, S. Vierrath and M. Breitwieser, Hydrocarbon-based Pemion™ proton exchange membrane fuel cells with state-of-the-art performance, *Sustainable Energy Fuels*, 2021, 3687–3699.

11 K. C. Neyerlin, H. A. Gasteiger, C. K. Mittelsteadt, J. Jorne and W. Gu, Effect of Relative Humidity on Oxygen Reduction Kinetics in a PEMFC, *J. Electrochem. Soc.*, 2005, **152**, A1073.

12 H. Xu, Y. Song, H. R. Kunz and J. M. Fenton, Effect of Elevated Temperature and Reduced Relative Humidity on ORR Kinetics for PEM Fuel Cells, *J. Electrochem. Soc.*, 2005, **152**, A1828.

13 D. Novitski and S. Holdcroft, Determination of O$_2$ Mass Transport at the Pt | PFSA Ionomer Interface under Reduced Relative Humidity, *ACS Appl. Mater. Interfaces*, 2015, **7**, 27314–27323.

14 H. Xu, H. R. Kunz and J. M. Fenton, Analysis of proton exchange membrane fuel cell polarization losses at elevated temperature 120 °C and reduced relative humidity, *Electrochim. Acta*, 2007, **52**, 3525–3533.

15 D. Novitski, Z. Xie and S. Holdcroft, Time-Dependent Mass Transport for O$_2$ Reduction at the Pt Perfluorosulfonic Acid Ionomer Interface, *ECS Electrochem. Lett.*, 2014, **4**, F9–F12.

16 A. S. Aricò, A. Di Blasi, G. Brunaccini, F. Sergi, G. Dispenza, L. Andaloro, M. Ferraro, V. Antonucci, P. Asher and S. Buche, *et al.*, High Temperature Operation of a Solid Polymer Electrolyte Fuel Cell Stack Based on a New Ionomer Membrane, *Fuel Cells*, 2010, **10**, 1013–1023.

17 J. Zhang, Y. Tang, C. Song, Z. Xia, H. Li, H. Wang and J. Zhang, PEM fuel cell relative humidity (RH) and its effect on performance at high temperatures, *Electrochim. Acta*, 2008, **53**, 5315–5321.

18 K. C. Neyerlin, W. Gu, J. Jorne, A. Clark and H. A. Gasteiger, Cathode Catalyst Utilization for the ORR in a PEMFC, *J. Electrochem. Soc.*, 2007, **154**, B279.

19 Q. Wang, M. Eikerling, D. Song, Z. Liu, T. Navessin, Z. Xie and S. Holdcroft, Functionally Graded Cathode Catalyst

Layers for Polymer Electrolyte Fuel Cells, *J. Electrochem. Soc.*, 2004, **151**, A950.

20 K. C. Hess, W. K. Epting and S. Litster, Spatially resolved, *in situ* potential measurements through porous electrodes as applied to fuel cells, *Anal. Chem.*, 2011, **83**, 9492–9498.

21 K. Kim, H. Kim, K. Lee, J. Jang, S. Lee, E. Cho, I. Oh and T. Lim, Effect of Nafion® gradient in dual catalyst layer on proton exchange membrane fuel cell performance, *Int. J. Hydrogen Energy*, 2008, **33**, 2783–2789.

22 Z. Xie, T. Navessin, K. Shi, R. Chow, Q. Wang, D. Song, B. Andreaus, M. Eikerling, Z. Liu and S. Holdcroft, Functionally Graded Cathode Catalyst Layers for Polymer Electrolyte Fuel Cells, *J. Electrochem. Soc.*, 2005, **152**, A1171.

23 M. Breitwieser, M. Klingele, S. Vierrath, R. Zengerle and S. Thiele, Tailoring the Membrane-Electrode Interface in PEM Fuel Cells: A Review and Perspective on Novel Engineering Approaches, *Adv. Energy Mater.*, 2018, **8**, 1701257.

24 O. Antoine, Y. Bultel, P. Ozil and R. Durand, Catalyst gradient for cathode active layer of proton exchange membrane fuel cell, *Electrochim. Acta*, 2000, **45**, 4493–4500.

25 H.-N. Su, S.-J. Liao and Y.-N. Wu, Significant improvement in cathode performance for proton exchange membrane fuel cell by a novel double catalyst layer design, *J. Power Sources*, 2010, **195**, 3477–3480.

26 U.S. Department of Energy. FuelCell Technical Team Roadmap. https://www.energy.gov/sites/prod/files/2017/11/f46/FCTT_Roadmap_Nov_2017_FINAL.pdf.

27 H. A. Gasteiger, S. S. Kocha, B. Sompalli and F. T. Wagner, Activity benchmarks and requirements for Pt, Pt-alloy, and non-Pt oxygen reduction catalysts for PEMFCs, *Appl. Catal., B*, 2005, **56**, 9–35.

28 H. Schulenburg, J. Durst, E. Müller, A. Wokaun and G. G. Scherer, Real surface area measurements of $Pt_3Co/C$ catalysts, *J. Electroanal. Chem.*, 2010, **642**, 52–60.

29 D. F. van der Vliet, C. Wang, D. Li, A. P. Paulikas, J. Greeley, R. B. Rankin, D. Strmcnik, D. Tripkovic, N. M. Markovic and V. R. Stamenkovic, Unique Electrochemical Adsorption Properties of Pt-Skin Surfaces, *Angew. Chem.*, 2012, **124**, 3193–3196.

30 P. A. Heizmann, H. Nguyen, M. von Holst, A. Fischbach, M. Kostelec, F. Javier Gonzalez Lopez, M. Bele, L. Pavko, T. Đukić and M. Šala, *et al.*, PtCo/C catalysts with narrow particle size distribution improve high current density operation in PEM fuel cells [Online early access], DOI: 10.26434/chemrxiv-2022-8k3dt.

31 I. Arganda-Carreras, V. Kaynig, C. Rueden, K. W. Eliceiri, J. Schindelin, A. Cardona and H. Sebastian Seung, Trainable Weka Segmentation: a machine learning tool for microscopy pixel classification, *Bioinformatics*, 2017, **33**, 2424–2426.

32 K.-H. Kim, K.-Y. Lee, H.-J. Kim, E. Cho, S.-Y. Lee, T.-H. Lim, S. P. Yoon, I. C. Hwang and J. H. Jang, The effects of Nafion® ionomer content in PEMFC MEAs prepared by a catalyst-coated membrane (CCM) spraying method, *Int. J. Hydrogen Energy*, 2010, **35**, 2119–2126.

33 A. Orfanidi, P. Madkikar, H. A. El-Sayed, G. S. Harzer, T. Kratky and H. A. Gaststeiger, The Key to High Performance Low Pt Loaded Electrodes, *J. Electrochem. Soc.*, 2017, **164**, F418–F426.

34 A. Suzuki, U. Sen, T. Hattori, R. Miura, R. Nagumo, H. Tsuboi, N. Hatakeyama, A. Endou, H. Takaba and M. C. Williams, *et al.*, Ionomer content in the catalyst layer of polymer electrolyte membrane fuel cell (PEMFC): Effects on diffusion and performance, *Int. J. Hydrogen Energy*, 2011, **36**, 2221–2229.

35 J. Xie, F. Xu, D. L. Wood, K. L. More, T. A. Zawodzinski and W. H. Smith, Influence of ionomer content on the structure and performance of PEFC membrane electrode assemblies, *Electrochim. Acta*, 2010, **55**, 7404–7412.

36 S. Sambandam, J. Parrondo and V. Ramani, Estimation of electrode ionomer oxygen permeability and ionomer-phase oxygen transport resistance in polymer electrolyte fuel cells, *Phys. Chem. Chem. Phys.*, 2013, 14994–15002.

37 K. Kodama, A. Shinohara, N. Hasegawa, K. Shinozaki, R. Jinnouchi, T. Suzuki, T. Hatanaka and Y. Morimoto, Catalyst Poisoning Property of Sulfonimide Acid Ionomer on Pt (111) Surface, *J. Electrochem. Soc.*, 2014, **161**, F649–F652.

38 K. Shinozaki, Y. Morimoto, B. S. Pivovar and S. S. Kocha, Suppression of oxygen reduction reaction activity on Pt-based electrocatalysts from ionomer incorporation, *J. Power Sources*, 2016, **325**, 745–751.

39 M. K. Sabbe, L. Laín, M.-F. Reyniers and G. B. Marin, Benzene adsorption on binary Pt3M alloys and surface alloys: a DFT study, *Phys. Chem. Chem. Phys.*, 2013, **15**, 12197–12214.

40 M. P. Soriaga and A. T. Hubbard, Determination of the orientation of adsorbed molecules at solid-liquid interfaces by thin-layer electrochemistry: aromatic compounds at platinum electrodes, *J. Am. Chem. Soc.*, 1982, **104**, 2735–2742.

41 I. Matanovic, S. Maurya, E. J. Park, J. Y. Jeon, C. Bae and Y. S. Kim, Adsorption of Polyaromatic Backbone Impacts the Performance of Anion Exchange Membrane Fuel Cells, *Chem. Mater.*, 2019, **31**, 4195–4204.

42 S. Kabir, D. J. Myers, N. Kariuki, J. Park, G. Wang, A. Baker, N. Macauley, R. Mukundan, K. L. More and K. C. Neyerlin, Elucidating the Dynamic Nature of Fuel Cell Electrodes as a Function of Conditioning: An ex Situ Material Characterization and in Situ Electrochemical Diagnostic Study, *ACS Appl. Mater. Interfaces*, 2019, **11**, 45016–45030.

43 H. A. Gasteiger, J. E. Panels and S. G. Yan, Dependence of PEM fuel cell performance on catalyst loading, *J. Power Sources*, 2004, **127**, 162–171.

44 K. C. Neyerlin, W. Gu, J. Jorne and H. A. Gasteiger, Determination of Catalyst Unique Parameters for the Oxygen Reduction Reaction in a PEMFC, *J. Electrochem. Soc.*, 2006, **153**, A1955.

45 A. Z. Weber and A. Kusoglu, Unexplained transport resistances for low-loaded fuel-cell catalyst layers, *J. Mater. Chem. A*, 2014, **2**, 17207–17211.